

# A versatile index to characterize hysteresis between hydrological variables at the runoff event timescale

G. Zuecco,<sup>1\*</sup> D. Penna,<sup>2</sup> M. Borga<sup>1</sup> and H. J. van Meerveld<sup>3</sup>

<sup>1</sup> Department of Land, Environment, Agriculture and Forestry, University of Padova, Padua, Italy

<sup>2</sup> Faculty of Science and Technology, Free University of Bozen-Bolzano, Bolzano, Italy

<sup>3</sup> Department of Geography, University of Zurich, Zurich, Switzerland

## Abstract:

This study presents a versatile index for the quantification of hysteretic loops between hydrological variables at the runoff event timescale. The conceptual development of the index is based on a normalization of the input data and the computation of definite integrals at fixed intervals of the independent variable. The sum, the minimum and the maximum of the differences between integrals computed for the rising and the falling curves provide information on the direction, the shape and the extent of the loop. The index was tested with synthetic data and field data from experimental catchments in Northern Italy. Hysteretic relations between streamflow (the independent variable) and soil moisture, depth to water table, isotopic composition and electrical conductivity of stream water (dependent variables) were correctly identified and quantified by the index. The objective quantification of hysteresis by the index allows for the automatic classification of hysteretic loops and thus the determination of differences in hydrological responses during different events. The index was also used to examine the seasonal dynamics in the relation between streamflow and soil moisture and captured the switch in the direction of the loop with changes in event size and antecedent wetness conditions. The sensitivity of the index to the temporal resolution of the measurements and measurement errors was also tested. The index can successfully quantify hysteresis, except for very noisy data or when the temporal resolution of the measurements is not well suited to study hysteresis between the variables. Copyright © 2015 John Wiley & Sons, Ltd.

KEY WORDS hysteresis index; streamflow; soil moisture; seasonal dynamics; sensitivity analysis

Received 23 October 2014; Accepted 25 August 2015

## INTRODUCTION

Hysteresis is a non-linear loop-like behaviour that is common in natural systems. Phillips (2003) defined hysteresis in geomorphic systems as a phenomenon where two or more values of a dependent variable are associated with a single value of an independent variable. Similarly, O’Kane (2005) suggested that hysteretic loops in hydrological systems could be seen as rate-dependent behaviours that do not show affine similarity with respect to time. In other words, when the time-argument of an input function is stretched or compressed, the corresponding output function is not stretched in the same way (O’Kane, 2005). Typically, this occurs when a time lag exists between the two variables (Prowse, 1984). Hysteresis can thus be thought of as the dependence of a response variable not only on the value of a driving variable but also on its past history (Camporese *et al.*, 2014; Norbiato and Borga, 2008; Visintin, 2006).

Hysteretic relations are common in hydrology. Hysteresis occurs in the relation between soil water content and pressure head (soil water retention curve) and between stream stage and streamflow during unsteady flow conditions. Hysteresis has also been identified in the relation between streamflow and a number of other hydrologic variables: precipitation (e.g. Andermann *et al.*, 2012), groundwater level (e.g. Fovet *et al.*, 2015; Camporese *et al.*, 2014; Allen *et al.*, 2010; Frei *et al.*, 2010), soil moisture content (e.g. Penna *et al.*, 2011; Parajka *et al.*, 2006), extent of the saturated area (e.g. Shook and Pomeroy, 2011; Niedzialek and Ogden, 2004), storage (e.g. Davies and Beven, 2015), hillslope flow (e.g. McGuire and McDonnell, 2010), sediment concentrations (both bedload and suspended sediment, e.g. Mao *et al.*, 2014; Landers and Sturm, 2013), solute concentrations (e.g. Burt *et al.*, 2015; Cartwright *et al.*, 2014; Outram *et al.*, 2014; Aubert *et al.*, 2013; Hornberger *et al.*, 2001; Evans and Davies, 1998) and stream water temperature (e.g. Blaen *et al.*, 2013; Subehi *et al.*, 2010). Hysteretic relations were also found between the diurnal variation in evapotranspiration and vapour pressure deficit (e.g. Zhang *et al.*, 2014; Zheng *et al.*, 2014), spatial mean

\*Correspondence to: Giulia Zuecco, Department of Land, Environment, Agriculture and Forestry, University of Padova, viale dell’Università 16, Agripolis, Legnaro, PD 35020, Italy.  
E-mail: giulia.zuecco@studenti.unipd.it

soil moisture and coefficient of variation (e.g. Fatichi *et al.*, 2015; Ivanov *et al.*, 2010), bulk and fluid electrical conductivity (e.g. Briggs *et al.*, 2014), air and river water temperature (e.g. Wilby *et al.*, 2014) and surface water cover and water storage (e.g. Kuppel *et al.*, 2015).

Analysis of hysteretic relations has led to a better understanding of the nonlinear mechanisms underlying runoff generation at various scales (Spence, 2010). The changing direction of the hysteretic relation between hillslope flow and streamflow (McGuire and McDonnell, 2010) and between hillslope soil moisture and streamflow (Penna *et al.*, 2011) highlighted the effect of antecedent soil moisture conditions on the timing of hillslope contributions to streamflow. Similarly, changes in the relation between streamflow and solute concentrations have been related to the different degrees of connectivity of hillslopes and stream tributaries (Murphy *et al.*, 2014) or different solute sources in the catchment (Shanley *et al.*, 2015). Differences in hysteresis in the relation between sediment concentrations and streamflow for different events or different catchments have been interpreted with respect to differences in the source area of the suspended sediment. Generally, clockwise hysteretic loops are related to a quick flushing of sediment close to the measuring station (e.g. Mano *et al.*, 2009). Aich *et al.* (2014) showed differences in hysteresis for a series of runoff events for a hillslope and the catchment outlet, providing valuable information about the differences in exhaustion of sediment sources, and seasonal changes in sediment detachment and transport. Numerical simulations showed that the hysteretic relation between sediment concentrations and flow depends on the particle size distribution of the soil and the presence of a deposited layer that protects the soil below (Sander *et al.*, 2011). Studying hysteretic relations for different events or differences in hysteretic patterns between different sites can thus reveal important information about the underlying hydrological processes.

Analysis of hysteretic patterns is typically carried out via a bivariate plot to highlight the relation between the response of one parameter to variations in another parameter. Hysteretic relations can also be described and analysed with indices or metrics that quantify the three main characteristics of hysteretic relations: (i) the shape (circular, eight-shaped or linear), (ii) the direction (clockwise or anticlockwise) and (iii) the extent of the loop. Quantitative indices are valuable tools to compare hysteretic loops at various space and time-scales, to develop a classification of hysteretic patterns, to detect changes in hysteretic loops or to test the ability of models to reproduce the observed hysteretic behaviour (Fovet *et al.*, 2015; Zhang *et al.*, 2014; Zheng *et al.*, 2014). In the past decade, several researchers have developed indices to quantify the shape, size and direction of hysteretic loops.

For instance, Poggi-Varaldo and Rinderknecht-Seijas (2003) analysed the hysteretic behaviour in adsorption–desorption and derived the hysteresis coefficient, defined as the ratio of the derivatives of the adsorption and desorption isotherms at a given point. Butturini *et al.* (2006) examined the temporal variation in hysteresis between streamflow and dissolved organic carbon and nitrate concentrations. Their index,  $\Delta R$ , integrated information about the area and the direction of the hysteretic loop and was obtained by standardizing streamflow and solute concentrations and multiplying the extent of the loop by the term  $R$  ( $R=1$  for clockwise loops,  $R=-1$  for anticlockwise loops and  $R=0$  for unclear patterns or a linear relation between streamflow and solute concentration) and then by 100. Therefore,  $\Delta R$  varied between  $-100$  (for large anticlockwise loops) and  $100$  (for large clockwise loops). Bieroza and Heathwaite (2015) successfully used this index to study the seasonal variation in hysteresis between streamflow and phosphorus concentrations. Several other methods for the quantification of hysteretic relations were based on measurements of suspended sediment concentrations and streamflow. Langlois *et al.* (2005) analysed suspended sediment transport dynamics during a snow-melt period in a small forested catchment in Nevada, USA. They plotted suspended sediment concentrations against streamflow and computed regression lines for the rising and falling limbs of the hydrograph. The area under the curve for the two regression equations was estimated by integration using the lowest streamflow and the maximum streamflow observed during the event as the lower and upper limits, respectively. The hysteresis index,  $H$ , was computed as the ratio of these two areas, where  $H \approx 1$  indicated weak hysteresis,  $H > 1$  a clockwise hysteretic loop and  $H < 1$  an anticlockwise hysteretic loop. Lawler *et al.* (2006) studied turbidity during spring storm events in an urban catchment in the UK and also developed a dimensionless index to quantify the magnitude and direction of hysteresis in the relationship between streamflow and turbidity. Their index was based on the extent of the hysteretic loop at the mid-point of streamflow during the event (i.e. halfway between baseflow prior to the event and peak streamflow). Interpolation was used to find the two turbidity values at the mid-point streamflow. The direction of hysteresis was expressed by the index  $HI_{mid}$  and based on a conditional statement: if turbidity on the rising limb was higher than on the falling limb, the loop was clockwise; otherwise, it was anticlockwise. Lawler *et al.* (2006) state that  $HI$  can also be computed for multiple streamflow points and then averaged ( $HI_{mean}$ , Lawler *et al.*, 2006). Smith and Dragovich (2009) developed a dimensionless similarity function based on individual line lengths and angles between the suspended sediment concentration and

streamflow for each sampling time. They used this index to study the similarity in the hysteretic patterns between suspended sediment concentrations and streamflow at the outlet of two nested catchments in South-Eastern Australia and showed that quantitative measures of hysteretic patterns at the event timescale provided a mechanism for linking the timing and magnitude of responses across spatial scales (Smith and Dragovich, 2009). Landers and Sturm (2013) used turbidity measurements to estimate suspended sediment concentrations in a mesoscale catchment in Georgia, USA. They quantified hysteresis between suspended sediment concentrations and streamflow and between suspended sediment concentrations and turbidity at the runoff event timescale by computing the range and coefficient of variation of the ratios of streamflow and turbidity to suspended sediment concentration. They based these calculations on the observation that, where hysteresis occurred, the magnitude of hysteresis (i.e. the nonlinearity in the bivariate plot) increased with increasing range and coefficient of variation of those ratios. Finally, Aich *et al.* (2014) normalized streamflow and sediment concentrations and computed the hysteresis index (*HI*) as the sum of the maximum distances between the rising and the falling limbs of the hysteretic loop and the line that links the streamflow peak to the last sediment concentration data point. *HI* was positive for clockwise hysteresis and negative for anticlockwise loops. They used this index to compare hysteresis in the relation between streamflow and suspended sediment concentrations at the catchment outlet and a hillslope.

The use of these previously developed indices provided detailed understanding of the processes investigated and proved to be useful for the specific cases for which they were developed. However, these indices also have some limitations. Some of them require a certain degree of subjectivity and personal interpretation during their application, which limits their robustness and their use for identifying changes in hysteretic patterns in long data series (e.g. Langlois *et al.*, 2005). They were also not developed to take into account more complex hysteretic patterns, such as eight-shaped loops that combine both clockwise and anticlockwise hysteresis (e.g. Aich *et al.*, 2014; Langlois *et al.*, 2005). In addition, some indices (e.g. Lawler *et al.*, 2006; Langlois *et al.*, 2005) cannot be used with negative data (e.g. delta values that describe the isotopic composition of streamflow). Finally, none of these studies provided a sensitivity analysis to verify the results of the index. Knowledge of the sensitivity of the index is needed when the index is used for long data series with many events to study seasonal changes in hysteresis, to compare hysteretic responses in different catchments or at different scales or to compare observed and modelled hysteretic relations, particularly




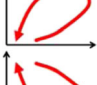



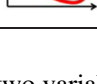
when noisy input data or different time intervals (temporal resolution) are used. Therefore, the objective of this paper is to introduce a versatile index for the quantification of a wide range of hysteretic loops at the runoff event timescale. Specifically, we (i) present an index that is able to predict the eight main hysteretic loop types, (ii) test the robustness and usefulness of the index using synthetic data and field data from experimental catchments in Northern Italy and (iii) assess the sensitivity of the index to noisy data and data with different temporal resolutions.

#### DEVELOPMENT OF THE HYSTERESIS INDEX

The index is developed for hysteretic loops where the independent variable ( $x(t)$ ) increases from its initial value, reaches a peak and then decreases. In hydrological applications, this is typically the case of streamflow, groundwater levels or soil moisture content, which increase during rainfall, snowmelt or glacier melt events and then decline. The dependent variable ( $y(t)$ ) can increase or decrease during the event. We assume that the evolution of the dependent variable is related to that of the independent variable. In the examples we report in the section on *Application to Field Data*, we investigate the relation between streamflow and other hydrological variables at the runoff event timescale, so that  $x$  is streamflow.

The index is based on the computation of definite integrals on the increasing and decreasing curve of the independent variable. We define the rising curve as the part of the curve of the independent variable that goes from the initial value to its highest value, and the falling curve as the part of the curve of the independent variable that goes from the peak to the last observed value. We use the last observed value as loops do not always close (i.e. the variables do not always return to their initial state). We define eight main hysteresis classes: clockwise (classes: I and V), anticlockwise (classes: IV and VIII) or eight-shaped (or more complex), where the main direction is clockwise (classes: II and VI) or anticlockwise (classes: III and VII) (Table I). Class I to IV describe the situation where the dependent variable mainly increases during the rising curve of the independent variable, while classes V–VIII describe the situation where the dependent variable mainly decreases during the rising curve of the independent variable. If the dependent variable remains constant during the rising curve of the independent variable, then the classification of the loops is based on whether the dependent variable mainly increases or decreases during the falling curve. The hysteresis index is structured so that it can classify hysteretic loops into these eight classes. The computation of the hysteresis index involves four steps, which were implemented in MATLAB scripts (MathWorks, Inc., Natick, MA, USA) and a stand-alone tool in Java and are available upon request:

Table I. The eight main hysteresis classes for independent variables that increase from the initial state, reach a peak and then decrease, with the corresponding minimum ( $\Delta A_{\min}$ ) and maximum ( $\Delta A_{\max}$ ) values of the difference between the integrals  $\Delta A_{[i,j]}$  (Equation 5) and their sum,  $h$

Hysteresis class	Loop	Dependent variable	$\Delta A_{\min}$	$\Delta A_{\max}$	$h$
I		Increases from the initial state	$>0$	$>0$	$>0$
II		Increases from the initial state	$\leq 0$	$>0$	$\geq 0$
III		Increases from the initial state	$<0$	$\geq 0$	$<0$
IV		Increases from the initial state	$<0$	$<0$	$<0$
V		Decreases from the initial state	$>0$	$>0$	$>0$
VI		Decreases from the initial state	$\leq 0$	$>0$	$\geq 0$
VII		Decreases from the initial state	$<0$	$\geq 0$	$<0$
VIII		Decreases from the initial state	$<0$	$<0$	$<0$

1. Normalization of the two variables (columns a and b in Figure 1), as

$$u(t) = \frac{x(t) - x_{\min}}{x_{\max} - x_{\min}} \tag{1}$$

$$v(t) = \frac{y(t) - y_{\min}}{y_{\max} - y_{\min}} \tag{2}$$

where  $x(t)$  and  $y(t)$  are the two variables at time  $t$ ;  $x_{\min}$ ,  $x_{\max}$ ,  $y_{\min}$  and  $y_{\max}$  are the minimum and maximum values of the independent and dependent variables, respectively; and  $u(t)$  and  $v(t)$  are the normalized values of  $x(t)$  and  $y(t)$ , respectively. The two normalized variables range between 0 and 1. Typically,  $x_{\min}$  should be the independent variable at its initial state, so that normally  $u(0) = 0$ .

2. Computation of the definite integrals,  $A_{r[i,j]}$  and  $A_{f[i,j]}$  of the functions  $v_r(u)$  and  $v_f(u)$  on intervals  $[i,j]$  for the rising (r) and the falling (f) curve, as

$$A_{r[i,j]} = \int_i^j v_r(u) du \tag{3}$$

$$A_{f[i,j]} = \int_i^j v_f(u) du \tag{4}$$

where  $i$  and  $j$  represent the lower and upper limits of integration, respectively, and can assume all the values from  $u = 0$  to  $u = 1$ . The integrals can be computed on intervals of different widths delimited by selected points,

$i$  and  $j$ , of the independent variable  $u$  (column c and d in Figure 1). The choice of the intervals of integrations should depend on the quality and resolution of the data and the rate at which the dependent variable changes with respect to the independent variable. In the examples in the section on *Application to Field Data*, we computed the integrals by subdividing the range from  $u = 0.15$  to  $u = 1$  into equal steps of 0.05 and using a linear interpolation. The definite integrals for the rising and the falling curves can be plotted as a function of  $u$  (column d in Figure 1). For clockwise loops, the integrals of the rising curve are always larger than the integrals of the falling curve (Figure 1 column d, hysteresis class I); for anticlockwise loops, the integrals of the falling curve are always larger than those of the rising curve (Figure 1 column d, hysteresis class IV), while for eight-shaped or other complex hysteretic loops, the integrals of the two curves cross (i.e. some integrals of the rising curve are larger than those on the falling curve, while others are smaller than those of the falling curve; Figure 1 column d, hysteresis classes II and III).

3. Determination of the differences between the definite integrals on the rising and the falling curves computed for the same interval,  $[i,j]$ , as

$$\Delta A_{[i,j]} = A_{r[i,j]} - A_{f[i,j]} \tag{5}$$

Clockwise loops have all  $\Delta A_{[i,j]} > 0$ , and anticlockwise loops have all  $\Delta A_{[i,j]} < 0$ , linear relations (no hysteresis)

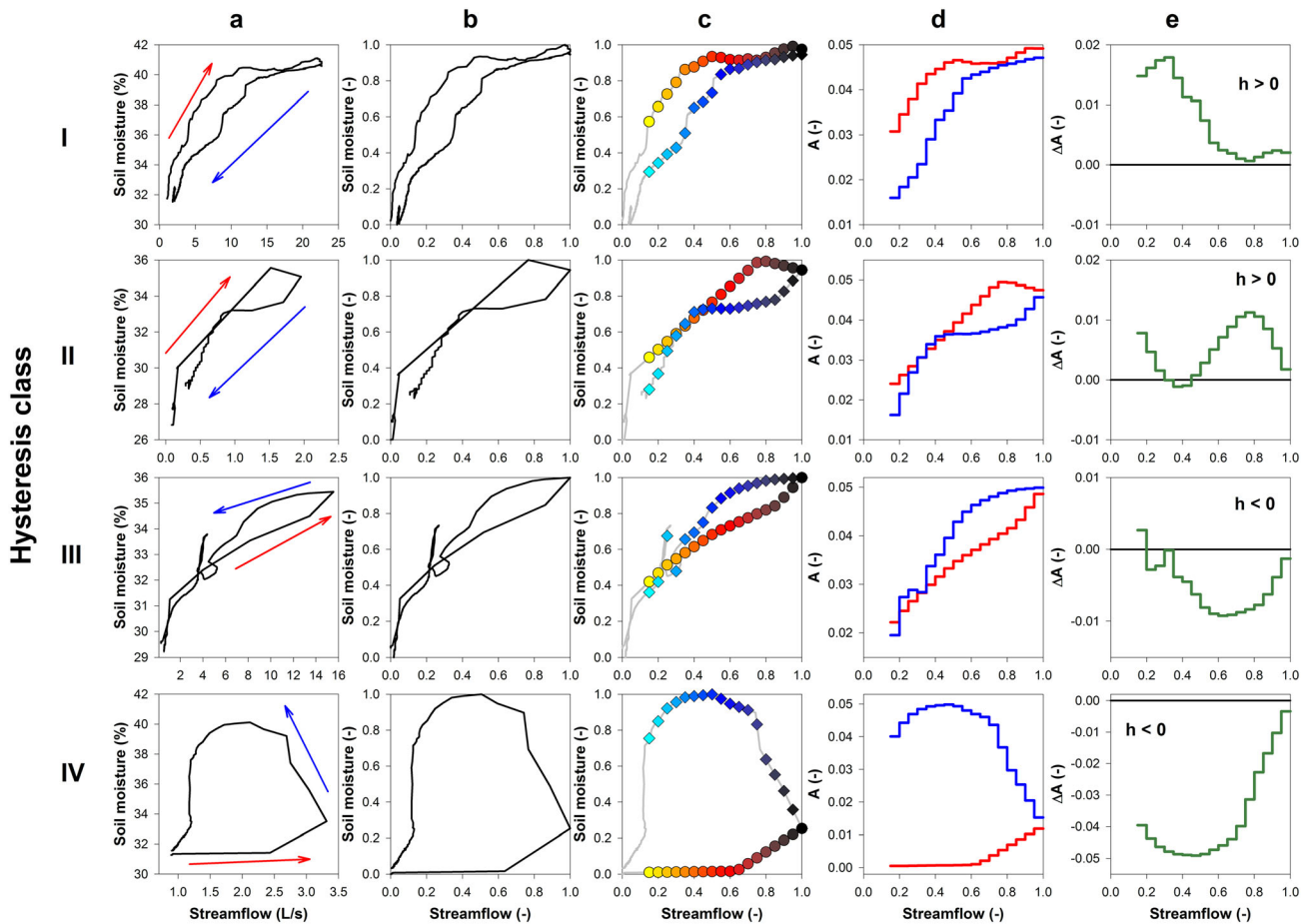


Figure 1. Examples of hysteretic relations between streamflow and soil moisture representing the four main hysteresis classes (column a) and the main steps in the computation of the hysteresis index (columns b–e). The circles and diamonds in column c represent the selected points ( $u$ ) delimiting the intervals of integration on the rising and the falling limbs, respectively. The symbol colours change from yellow to dark red to cyan during the runoff event. The horizontal black line in column e represents  $\Delta A = 0$

have all  $\Delta A_{[i,j]} = 0$ , while eight-shaped hysteretic patterns are characterized by  $\Delta A_{\min} < 0$  and  $\Delta A_{\max} > 0$  (column e in Figure 1 and Table I), where  $\Delta A_{\min}$  and  $\Delta A_{\max}$  are the minimum and maximum values of  $\Delta A_{[i,j]}$ , respectively.

3. Quantification of the  $h$  index, as

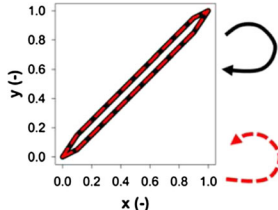
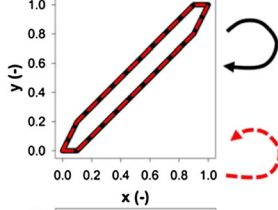
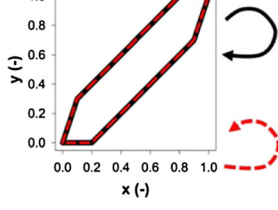
$$h = \sum_{k=1}^n \Delta A_{[i,j]} \quad (6)$$

where  $n$  is the number of intervals ( $n = 17$  in the examples in the section on *Application to Field Data*). Clockwise hysteresis is characterized by  $h > 0$ , and anticlockwise loops have  $h < 0$ , while  $h \approx 0$  indicates no hysteresis or a symmetrical eight-shaped or complex loop (Table I). For complex eight-shaped loops, the dominant direction is defined by the relative size of the two (or more) loops. The value of the index is also a measure of the size of the hysteretic loop: the larger the hysteretic loop, the further  $h$  is from 0.

APPLICATION TO SYNTHETIC DATA

We used synthetic loops to test the ability of the hysteresis index  $h$ ,  $\Delta A_{\min}$  and  $\Delta A_{\max}$  to quantify the direction and the size of the loops. We also compared the index to (i) the  $H$  index developed by Langlois *et al.* (2005), (ii)  $HI_{\text{mid}}$  computed according to Lawler *et al.* (2006) and (iii) its modified version,  $HI_{\text{mean}}$ , where instead of using the ratio of the dependent variable at the mid-point of  $x$ , the ratio is averaged for multiple pairs, and (iv) the  $HI$  index developed by Aich *et al.* (2014) (Tables II and III). We set equal-width intervals of 0.05, from  $u = 0$  to  $u = 1$ , for the computation of  $h$ . The selected independent variable points for the computation of  $HI_{\text{mean}}$  were similarly set from 0.05 to 0.95 in equal intervals of 0.05. The results show that the  $h$  index, the  $H$  index developed by Langlois *et al.* (2005), the  $HI$  index developed by Aich *et al.* (2014) and  $HI_{\text{mid}}$  developed by Lawler *et al.* (2006) were able to detect the direction of the loops correctly (clockwise or anticlockwise) (Table II).  $h$ ,  $HI_{\text{mid}}$  (Lawler

Table II. Synthetic loops with a different area (A, B, C) and direction (clockwise: black solid line, subscript 1; anticlockwise: red dashed line, subscript 2) used for testing the hysteresis indices and the corresponding values of  $h$  (Equation 6), the  $H$  index developed by Langlois *et al.* (2005), the  $HI_{mid}$  and  $HI_{mean}$  indices of Lawler *et al.* (2006) and the  $HI$  index of Aich *et al.* (2014)

		$h$	$H$	$HI_{mid}$	$HI_{mean}$	$HI$
		This study	Langlois <i>et al.</i> (2005)	Lawler <i>et al.</i> (2006)	Lawler <i>et al.</i> (2006)	Aich <i>et al.</i> (2014)
	A <sub>1</sub>	0.09	1.20	0.22	0.47	0.07
	A <sub>2</sub>	-0.09	0.83	-0.22	-0.47	-0.07
	B <sub>1</sub>	0.18	1.44	0.50	*	0.14
	B <sub>2</sub>	-0.18	0.69	-0.50	*	-0.14
	C <sub>1</sub>	0.34	2.03	1.33	*	0.28
	C <sub>2</sub>	-0.34	0.49	-1.33	*	-0.28

\*The index was affected by a division that included a zero (either in the numerator or in the denominator).

*et al.*, 2006) and  $HI$  (Aich *et al.*, 2014) also provided symmetry across the range of clockwise and anticlockwise hysteretic loops.  $HI_{mean}$  (Lawler *et al.*, 2006) was also able to detect the direction correctly, but the index was affected by the presence of at least one value of zero in the ratio (either in the numerator or denominator) (Table II). In hydrological applications, the dependent variable can be equal to zero (e.g. water table, isotopic composition or tracer concentration) or not change from its initial value; therefore, methods that are not sensitive to this are preferable.

We also tested the indices for synthetic eight-shaped loops (Table III). The methods for the computation of  $H$  (Langlois *et al.*, 2005),  $HI_{mid}$  (Lawler *et al.*, 2006) and  $HI$  (Aich *et al.*, 2014) do not give information about complex loops, but the indices were able to detect the perfect symmetry ( $H=1$ ,  $HI_{mid}=0$  and  $HI=0$ ) for the symmetric loops (B<sub>1</sub> and B<sub>2</sub> in Table III). The index  $h$  and the associated values of  $\Delta A_{min}$  and  $\Delta A_{max}$  can characterize the direction correctly for the eight-shaped loops with an identifiable main direction (A<sub>1</sub>, A<sub>2</sub>, C<sub>1</sub>, C<sub>2</sub>, D<sub>1</sub>, D<sub>2</sub>, E<sub>1</sub> and E<sub>2</sub> in Table III) and identify the symmetry of the shape (B<sub>1</sub> and B<sub>2</sub>). The values of  $HI_{mean}$  were different for B<sub>1</sub> and B<sub>2</sub> because the computation is based on ratios, which

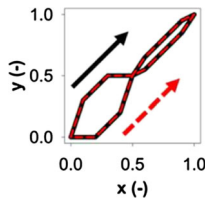
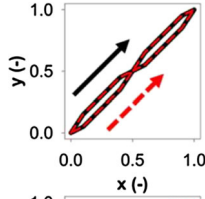
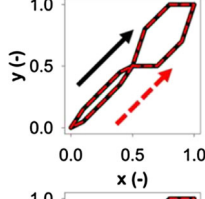
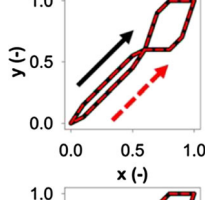
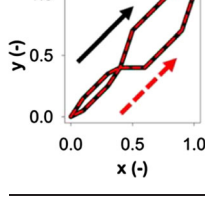
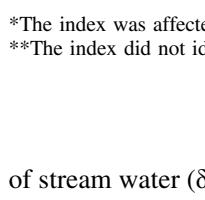
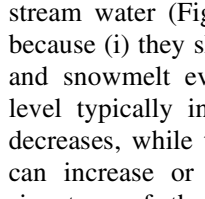
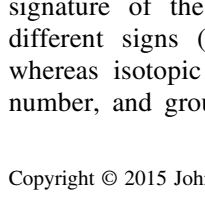

do not perfectly identify the symmetry of the shape. The comparison of the loops with the same area and main direction but with a different location of the largest loop (i.e. A<sub>1</sub> and C<sub>2</sub>, and A<sub>2</sub> and C<sub>1</sub>) shows that the value of  $HI_{mean}$  depends on the position of the largest portion of the loop (i.e. close or far from the peak of  $x$ ) and the skewness of the distribution of the ratios (D<sub>1</sub> and D<sub>2</sub> in Table III). The values of  $h$ ,  $H$ ,  $HI_{mid}$  and  $HI_{mean}$  reflected the different areas of the loops (e.g. C<sub>2</sub>, D<sub>2</sub> and E<sub>2</sub> and C<sub>1</sub>, D<sub>1</sub> and E<sub>1</sub> in Table III) and thus the differences in the extent of hysteresis. On the contrary,  $HI$  (Aich *et al.*, 2014) did not detect differences in the shape or the extent of the loops.

### APPLICATION TO FIELD DATA

#### *Instrumentation and datasets used to test the hysteresis index*

We tested the hysteresis index with hydrological data from three experimental catchments in Italy (Figure S1). We applied the index to the hysteretic relation between streamflow and four typical runoff response variables: soil moisture, depth to water table, isotopic composition

Table III. The synthetic eight-shaped loops used for testing the hysteresis indices with the values of  $h$ , the  $H$  index developed by Langlois *et al.* (2005), the  $HI_{mid}$  and  $HI_{mean}$  indices developed by Lawler *et al.* (2006) and the  $HI$  index of Aich *et al.* (2014). The arrows indicate the starting points of the loops: for values of  $x$  close to 0 on the rising limb, the black solid loops (subscript 1) have larger values of  $y$  compared with the red dashed loops (subscript 2).

	$h$	$H$	$HI_{mid}$	$HI_{mean}$	$HI$	
	This study	Langlois <i>et al.</i> (2005)	Lawler <i>et al.</i> (2006)	Lawler <i>et al.</i> (2006)	Aich <i>et al.</i> (2014)	
	A <sub>1</sub>	0.10	1.22**	0.00**	*	0.28**
	A <sub>2</sub>	-0.10	0.82**	0.00**	*	-0.28**
	B <sub>1</sub>	0.00	1.00**	0.00**	0.32	0.00**
	B <sub>2</sub>	0.00	1.00**	0.00**	-0.32	0.00**
	C <sub>1</sub>	-0.10	0.82**	0.00**	0.13	-0.28**
	C <sub>2</sub>	0.10	1.22**	0.00**	-0.13	0.28**
	D <sub>1</sub>	-0.05	0.90**	0.22**	0.24	-0.28**
	D <sub>2</sub>	0.05	1.11**	-0.22**	-0.24	0.28**
	E <sub>1</sub>	-0.15	0.74**	-0.75**	-0.03	-0.28**
	E <sub>2</sub>	0.15	1.35**	0.75**	0.03	0.28**

\*The index was affected by a division that included a zero (either in the numerator or in the denominator).

\*\*The index did not identify the eight-shaped loop.

of stream water ( $\delta^2H$ ) and electrical conductivity (EC) of stream water (Figure 2). These variables were chosen because (i) they show different responses during rainfall and snowmelt events (soil moisture and groundwater level typically increase during the event, EC usually decreases, while the stream water isotopic composition can increase or decrease depending on the isotopic signature of the rain or snowmelt); (ii) they have different signs (soil moisture and EC are positive, whereas isotopic composition is generally a negative number, and groundwater level can be positive, water

level above the bottom of the well, or negative, distance from the surface); and (iii) previous studies have shown a hysteretic relation between these variables and streamflow (Penna *et al.*, 2011; McGlynn *et al.*, 2004; Wetzel, 2003).

In order to apply the hysteresis index to the field data (Figure 2), we selected equal intervals of 0.05 from  $u=0.15$  to  $u=1$  on the rising and the falling curves. The number of selected intervals represents a reasonable frequency for the applications, leaving out possible noise for low flow observations ( $u < 0.15$ ). The use of different intervals did not change the results. Linear interpolation

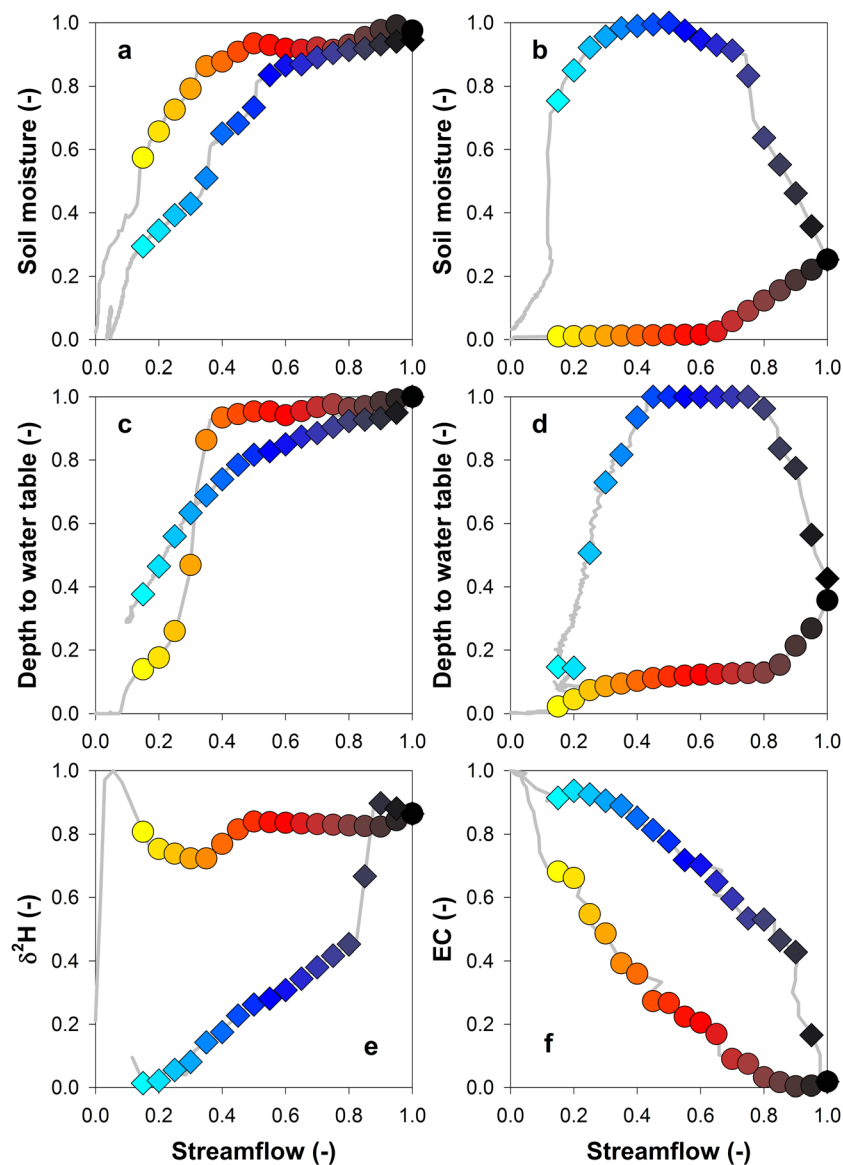


Figure 2. Normalized hysteretic loops between streamflow and soil moisture in the Ressi catchment (a: clockwise; b: anticlockwise), depth to water table in a piezometer in the Bridge Creek catchment (c: eight-shaped; d: anticlockwise),  $\delta^2\text{H}$  in streamflow in the Ressi catchment (e: eight-shaped) and the Electrical Conductivity (EC) in streamflow in the Alta Val de La Mare catchment (f: anticlockwise). Values of  $\Delta A_{\min}$ ,  $\Delta A_{\max}$  and  $h$  are reported in Table IV. Circles and diamonds represent selected points delimiting the 0.05 intervals of integration on the rising and the falling curves, respectively. The symbol colours change from yellow to dark red to cyan during the runoff event. See Figure S2 for the time series

between two observations was used to determine the corresponding values of the dependent variable,  $v(u)$  when data for the dependent variable at the selected times of  $h$  were missing in the dataset (i.e. the time stamp of the two datasets was not exactly the same).

*Ressi catchment.* Soil moisture and streamflow data were collected in the Ressi catchment ( $45^{\circ}47'11.79''\text{N}$ ,  $11^{\circ}15'54.12''\text{E}$ ; Italian pre-Alps) for 30 rainfall–runoff events (event total precipitation larger than 10 mm) between August 2012 and July 2013 (Penna *et al.*, 2015b). Precipitation amount ranged between 11.8 and

266.2 mm, while event-average rainfall intensity varied between 2.0 and 11.1 mm/h. Soil moisture was measured at 0–30 cm depth by four time domain reflectometres installed at different positions along a transect: SM1 was positioned in the riparian zone, SM2 at the transition between the riparian zone and the hillslope, SM3 in the middle part of the hillslope and SM4 in the upper part of the hillslope (for details, see Penna *et al.*, 2015b). Soil moisture was measured at a 5-min interval from mid-August 2012 until the end of November 2012, when the resolution was changed to 10 min. Stream stage was measured at a 5-min resolution by a pressure transducer



behind a V-notch weir. Streamflow was determined by the weir equation, which was checked by manual discharge measurements. The increase in streamflow (i.e. the difference between the minimum and maximum streamflow during an event) varied between 0.4 and 63.1 l/s for the 30 rainfall–runoff events. Because of the fast streamflow response, we analysed the rainfall–runoff events using a 5-min resolution data for both streamflow and soil moisture. Therefore, we used linear interpolation to estimate soil moisture at 5-min intervals from December 2012 to July 2013, when 5-min time resolution data were not available (17 out of the 30 events). We used the streamflow–soil moisture relation (Figure 2a, b) to evaluate the temporal variability of  $h$ , as well as the classification of the hysteretic loops, and their relation to event characteristics (e.g. average and maximum rainfall intensity, rainfall depth and runoff coefficient) and the antecedent soil moisture index ( $ASI$ ):

$$ASI = \theta \times D \tag{7}$$

where  $\theta$  is the volumetric soil moisture content ( $\text{m}^3/\text{m}^3$ ) measured by each probe and  $D$  is the installation depth (0.3 m) (Haga *et al.*, 2005; Detty and McGuire, 2010a, b). The correlation between the hysteresis index and the rainfall event characteristics was assessed using Spearman rank correlation analysis ( $\rho_s$ ).

In addition to the soil moisture data, we also tested the index for the hysteretic relation between streamflow and the isotopic composition of stream water during a 50-mm rainfall event on 5 May 2013 (Figure 2e). Additional information on water sampling and determination of the isotopic composition can be found in the study by Penna *et al.* (2015b).

*Bridge Creek catchment.* Figures 2c shows the hysteretic relation between streamflow and depth to water table measured with a pressure transducer in a piezometer on a hillslope during a 49-mm rain-on-snow event on 4 November 2012 at the Bridge Creek catchment (BCC, 46°29'32.34"N, 11°50'38.66"E; Eastern Italian Alps). Figure 2d shows the hysteretic relation between streamflow and depth to water table in a different

piezometer (125 m away) measured with a capacitance sensor during a 20-mm rainfall event on 5 August 2011. Stream stage at BCC was measured behind a V-notch weir with a pressure transducer. Streamflow was obtained by the weir equation, which was checked with bucket measurements. All data were collected at a 15-min interval. Information on the catchment and a detailed description of the groundwater responses can be found in Penna *et al.* (2011; 2015a).

*Alta Val de La Mare catchment.* Figure 2f shows the hysteretic relation between streamflow and stream water EC for a snowmelt event in the Noce Nero, a stream fed by snowmelt and spring water (Alta Val de La Mare catchment, 46°24'51.30"N, 10°40'50.90"E; Eastern Italian Alps, Carturan *et al.*, 2012). Stream stage and EC were measured at a 15-min interval by a Dipper-PTEC (SEBA Hydrometrie GmbH & Co., Germany) multi-parameter sensor. Streamflow was measured during different flow conditions using the salt dilution method.

*Identification of the different hysteretic relations*

The hysteresis index correctly represented the type of hysteretic loop: the clockwise loop (Figure 2a) had  $h > 0$ , and the anticlockwise loops (Figure 2b, d and f) had  $h < 0$  (Table IV). The range of  $\Delta A_{[i,j]}$  confirmed that the clockwise loop had all  $\Delta A_{[i,j]} > 0$ , the anticlockwise loops had all  $\Delta A_{[i,j]} < 0$  and the eight-shaped hysteretic patterns were characterized by  $\Delta A_{\min} < 0$  and  $\Delta A_{\max} > 0$  (Table IV). In particular, the values of  $\Delta A_{\min}$  and  $\Delta A_{\max}$  were useful to identify the eight-shaped loops (Figure 2c and e), where a small change in the hysteretic pattern occurred near the streamflow peak.

We also computed the indices developed by Langlois *et al.* (2005), Lawler *et al.* (2006) and Aich *et al.* (2014) for the six examples (Table V). The three indices captured the direction of the loops correctly when the dependent variables were expressed by positive signs. The direction of the loops with dependent variables with a negative sign (Figure 2c–e) was not correctly identified without any additional normalization or conditional statements:  $H$ ,  $HI_{\text{mid}}$  and  $HI_{\text{mean}}$  gave a wrong interpretation of

Table IV. Independent and dependent variables, sign of the dependent variable, hysteresis classes (Table I) and values of  $\Delta A_{\min}$ ,  $\Delta A_{\max}$  and  $h$  for the examples shown in Figure 2

Examples in Figure 2	Variables (x; y)	Sign of dependent variable	Hysteresis class	$\Delta A_{\min}$ (–)	$\Delta A_{\max}$ (–)	$h$ (–)
a	Streamflow; soil moisture	+	I	0.001	0.018	0.128
b	Streamflow; soil moisture	+	IV	–0.049	–0.003	–0.634
c	Streamflow; water table	–	II	–0.015	0.009	0.021
d	Streamflow; water table	–	IV	–0.044	–0.006	–0.567
e	Streamflow; $\delta^2\text{H}$	–	II	–0.003	0.038	0.383
f	Streamflow; EC	+	VIII	–0.026	–0.004	–0.360

Table V. Values for  $H$  (Langlois *et al.*, 2005),  $HI_{mid}$  (Lawler *et al.* (2006) and  $HI$  (Aich *et al.*, 2014) with notes about the interpretation of the direction of the hysteretic loops for the examples shown in Figure 2. The indices were applied without additional conditional statements or normalizations of the data. The values for  $\Delta A_{min}$ ,  $\Delta A_{max}$  and  $h$  are shown in Table IV

Examples in Figure 2	Hysteresis class	$H$ Langlois <i>et al.</i> (2005)	$HI_{mid}$ Lawler <i>et al.</i> (2006)	$HI$ Aich <i>et al.</i> (2014)
a	I	1.040 (correct)	0.050 (correct)	0.051 (correct)
b	IV	0.843 (correct)	-0.277 (correct)	-0.227 (correct)
c	II	1.011 (theoretically incorrect because of the negative sign of the dependent variable; difficult interpretation because it is an eight-shaped loop)	-0.101 (theoretically incorrect because of the negative sign of the dependent variable; no information about the eight shape)	-0.136 (correct for the normalized loop, but the normalization reverses the original loop; no information about the eight shape)
d	IV	1.475 (incorrect because of the negative sign of the dependent variable)	0.407 (incorrect because of the negative sign of the dependent variable)	0.734 (correct for the normalized loop, but the normalization reverses the direction of the original loop)
e	II	0.900 (incorrect because of the negative sign of the dependent variable; the correlation coefficient <0.90; difficult interpretation because it is an eight-shaped loop)	-0.111 (incorrect because of the negative sign of the dependent variable; no information about the eight shape)	-0.269 (correct for the normalized loop, but the normalization reverses the direction of the original loop; no information about the eight shape)
f	VIII	0.983 (correct)	-0.026 (correct)	-0.029 (correct)

the direction, while  $HI_{mean}$  gave a correct interpretation of the direction, but the normalization procedure reversed the loop. Eight-shaped hysteretic loops (Figure 2c and e) could not be correctly detected by any of these previous indices.

*Temporal variability in the hysteretic relation between soil moisture and streamflow*

The application of the hysteresis index to soil moisture and streamflow data for 30 events in the Ressi catchment showed that hysteretic loops between streamflow and

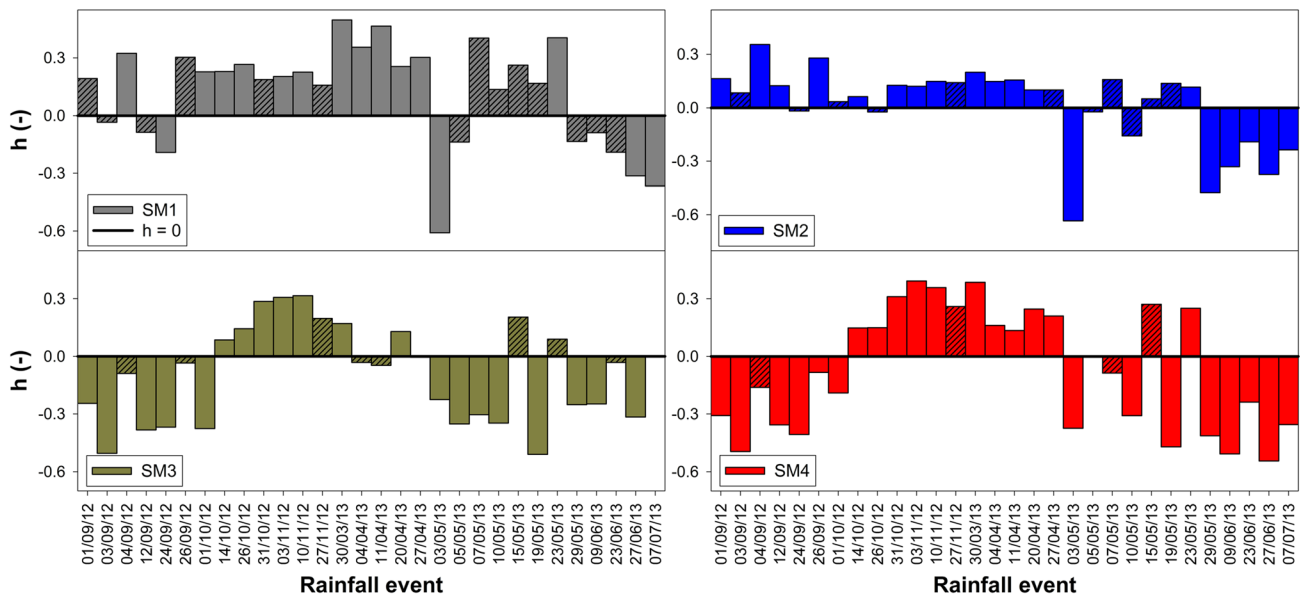


Figure 3. Values of the hysteresis index ( $h$ ) computed for the streamflow–soil moisture relations at four different locations (SM1: riparian zone; SM2: footslope; SM3: midslope; SM4: upper hillslope) in the Ressi catchment. The horizontal black line represents the threshold between mainly clockwise ( $>0$ ) and anticlockwise ( $<0$ ) loops. Shaded bars indicate eight-shaped or complex loops

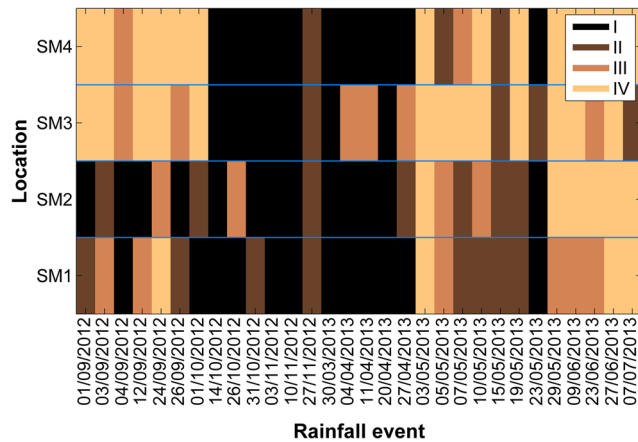


Figure 4. The hysteresis classes for the 30 rainfall–runoff events for the relation between streamflow and soil moisture at four different locations along the riparian-hillslope transect in Ressi (SM1: riparian zone; SM2: footslope; SM3: midslope; SM4: upper hillslope; I = clockwise loop; II = eight-shaped or complex loop with a predominant clockwise loop; III = eight-shaped or complex loop with a predominant anticlockwise loop; IV = anticlockwise loop)

riparian soil moisture (SM1 and SM2, Figure 3) were generally clockwise, with a few anticlockwise loops for events in May and June 2013. Conversely, hysteretic relations between streamflow and hillslope soil moisture (SM3 and SM4, Figure 3) followed a seasonal pattern, with clockwise loops during large events in autumn and anticlockwise loops occurring more commonly in spring and summer. Differences in the type of hysteretic loop for the hillslope and the riparian zone were most pronounced in late summer and late spring and smaller during wet periods (autumn 2012 and early spring 2013) and at the

start of the dry season (end of May 2013) (Figure 4). Because previous studies showed a threshold relation between streamflow and the sum of antecedent soil moisture and total rainfall (ASI+P) at the Ressi catchment (Penna *et al.*, 2015b), we investigated the relation between ASI+P and  $h$  for the four soil moisture measurement locations. The hysteresis index  $h$  for the hillslope sites was significantly correlated with ASI+P ( $\rho_s=0.69$  and  $0.73$  for SM3 and SM4, respectively,  $p<0.01$ ,  $n=30$ ) and also with event rainfall amount ( $\rho_s=0.72$  and  $0.73$  for SM3 and SM4, respectively,

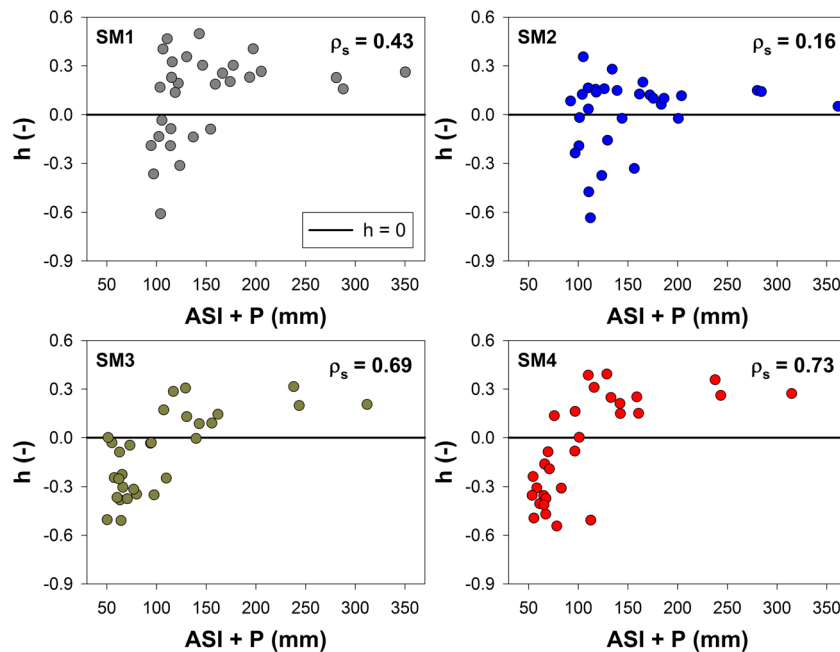


Figure 5. Relation between the value of the hysteresis index ( $h$ ) for the relation between streamflow and soil moisture and the antecedent soil moisture index plus precipitation (ASI+P) for the different locations along the riparian-hillslope transect at the Ressi catchment. The horizontal black line represents the threshold between the mainly clockwise ( $>0$ ) and anticlockwise ( $<0$ ) loops

Table VI. Frequency of the 30 rainfall–runoff events belonging to the four hysteresis classes (I–IV) for the observed data and for data with a 10- (a), 15- (b), 20- (c) and 30-min (d) temporal resolution, as well as the percentage of loops from a certain class that were reclassified to that class when the temporal resolution of the data was changed (italic font in inner square). For instance, 83.3% of the type III loops based on the original 5-min data were still characterized as a type III loop when using 10-, 15- or 20-min data (panel a, b and c, respectively), while 16.7% of the type III loops were reclassified as a type II loop using 10-, 15- or 20-min data (panel a, b and c, respectively). See Table I for the definition of the hysteresis classes.

a		Frequency 5 min data (%)				b		Frequency 5 min data(%)			
		I	II	III	IV			I	II	III	IV
Frequency 10 min data (%)		23.3	13.3	20.0	43.3	Frequency 15 min data (%)		23.3	13.3	20.0	43.3
I	23.3	<i>100.0</i>	<i>0.0</i>	<i>0.0</i>	<i>0.0</i>	I	23.3	<i>100.0</i>	<i>0.0</i>	<i>0.0</i>	<i>0.0</i>
II	13.3	<i>0.0</i>	<i>75.0</i>	<i>16.7</i>	<i>0.0</i>	II	13.3	<i>0.0</i>	<i>75.0</i>	<i>16.7</i>	<i>0.0</i>
III	23.3	<i>0.0</i>	<i>25.0</i>	<i>83.3</i>	<i>7.7</i>	III	23.3	<i>0.0</i>	<i>25.0</i>	<i>83.3</i>	<i>7.7</i>
IV	40.0	<i>0.0</i>	<i>0.0</i>	<i>0.0</i>	<i>92.3</i>	IV	40.0	<i>0.0</i>	<i>0.0</i>	<i>0.0</i>	<i>92.3</i>

c		Frequency 5 min data (%)				d		Frequency 5 min data (%)			
		I	II	III	IV			I	II	III	IV
Frequency 20 min data (%)		23.3	13.3	20.0	43.3	Frequency 30 min data (%) *		23.3	13.3	20.0	43.3
I	23.3	<i>100.0</i>	<i>0.0</i>	<i>0.0</i>	<i>0.0</i>	I	26.7	<i>100.0</i>	<i>0.0</i>	<i>16.7</i>	<i>0.0</i>
II	13.3	<i>0.0</i>	<i>75.0</i>	<i>16.7</i>	<i>0.0</i>	II	10.0	<i>0.0</i>	<i>75.0</i>	<i>0.0</i>	<i>0.0</i>
III	20.0	<i>0.0</i>	<i>0.0</i>	<i>83.3</i>	<i>7.7</i>	III	16.7	<i>0.0</i>	<i>25.0</i>	<i>66.7</i>	<i>0.0</i>
IV	43.3	<i>0.0</i>	<i>25.0</i>	<i>0.0</i>	<i>92.3</i>	IV	40.0	<i>0.0</i>	<i>0.0</i>	<i>16.7</i>	<i>84.6</i>

\*The hysteresis index  $h$  was computed for 28 instead of 30 rainfall–runoff events because the application of the different temporal resolution data resulted in the removal of the data point on the falling limb that corresponded to  $u = 0.15$ .

$p < 0.01$ ,  $n = 30$ ). The hysteretic relation between hillslope soil moisture and streamflow tended to be clockwise for high values of ASI+P and anticlockwise hysteresis for dry conditions and small events (Figure 5). These seasonal changes in the direction of hysteresis suggest that streamflow generally peaked before hillslope soil moisture during dry periods and small rainfall events, while hillslope soil moisture peaked earlier than streamflow during the wet period. Runoff coefficients were also positively correlated with  $h$ , with stronger correlations for the hillslope than the riparian zone [ $\rho_s = 0.50, 0.33, 0.67$  and  $0.86$  for SM1 ( $p < 0.01$ ), SM2 ( $p < 0.10$ ), SM3 ( $p < 0.01$ ) and SM4 ( $p < 0.01$ ), respectively,  $n = 30$ ].

The relation between  $h$  and ASI+P for the riparian sites was more scattered than for the hillslope sites [ $\rho_s = 0.43$  and  $0.16$  for SM1 ( $p < 0.05$ ) and SM2 ( $p > 0.10$ ), respectively,  $n = 30$ ], suggesting that hysteresis between streamflow and riparian soil moisture was not predominantly related to antecedent wetness conditions and rainfall amount. Instead, the hysteresis index for the relation between streamflow and riparian soil moisture at SM1 was negatively correlated with the average ( $\rho_s = -0.52$ ,  $p < 0.01$ ,  $n = 30$ ) and maximum rainfall intensity ( $\rho_s = -0.55$ ,  $p < 0.01$ ,  $n = 30$ ), implying that the time lag between streamflow and soil moisture decreased during high rainfall intensity events.

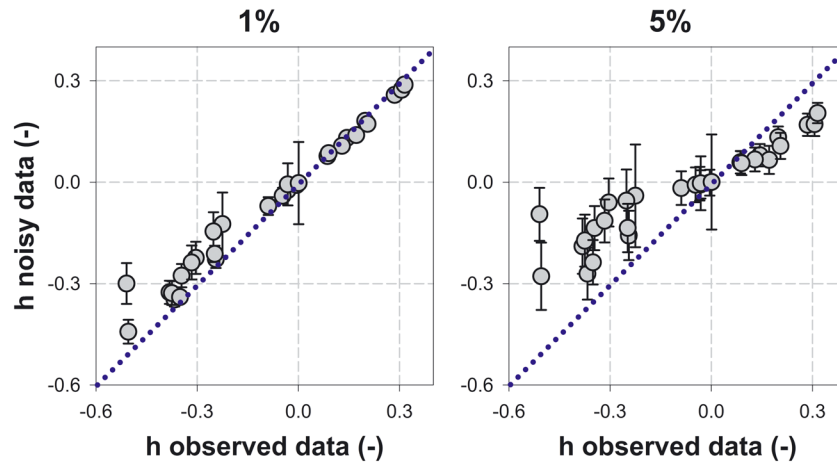


Figure 6. Simulated and observed values of  $h$  for the relation between streamflow and soil moisture at the midslope location (SM3) in Ressi catchment for the 30 studied rainfall–runoff events. Random instrumental noise was simulated 1000 times with a scaling factor of 1% (left) and 5% (right). The dots represent the median of the 1000 simulations, and the error bars represent the interquartile range

Table VII. The hysteresis class assigned using the measured data and the frequency of the hysteresis classes (I–IV) for the 1000 simulations with noisy data for each rainfall event with a 1% and 5% scaling factor. Bold values indicate the most frequently assigned hysteresis class with the noisy data for each rainfall event. See Table I for the definition of the hysteresis classes

Rainfall event	Class original data	1% scaling factor Frequency (%)				5% scaling factor Frequency (%)			
		I	II	III	IV	I	II	III	IV
01/09/12	IV	0.0	0.0	0.0	<b>100.0</b>	0.0	0.1	35.7	<b>64.2</b>
03/09/12	IV	0.0	0.0	0.0	<b>100.0</b>	0.0	0.0	13.9	<b>86.1</b>
04/09/12	III	0.0	0.1	<b>99.8</b>	0.1	0.0	33.3	<b>66.5</b>	0.2
12/09/12	IV	0.0	0.0	0.7	<b>99.3</b>	0.0	0.0	<b>51.4</b>	48.6
24/09/12	IV	0.0	0.0	0.0	<b>100.0</b>	0.0	0.0	4.5	<b>95.5</b>
26/09/12	III	0.0	3.2	<b>96.8</b>	0.0	0.1	44.0	<b>55.9</b>	0.0
01/10/12	IV	0.0	0.0	0.0	<b>100.0</b>	0.0	0.3	<b>51.2</b>	48.5
14/10/12	I	<b>91.4</b>	8.6	0.0	0.0	9.6	<b>89.7</b>	0.7	0.0
26/10/12	I	<b>74.7</b>	25.3	0.0	0.0	10.0	<b>89.8</b>	0.2	0.0
31/10/12	I	<b>100.0</b>	0.0	0.0	0.0	<b>52.9</b>	47.1	0.0	0.0
03/11/12	I	<b>99.8</b>	0.2	0.0	0.0	46.8	<b>53.2</b>	0.0	0.0
10/11/12	I	<b>95.5</b>	4.5	0.0	0.0	<b>52.2</b>	47.8	0.0	0.0
27/11/12	II	5.9	<b>94.1</b>	0.0	0.0	16.7	<b>83.3</b>	0.0	0.0
30/03/13	I	<b>75.4</b>	24.6	0.0	0.0	3.0	<b>94.7</b>	2.3	0.0
04/04/13	III	0.0	2.5	<b>96.5</b>	1.0	0.0	41.8	<b>58.2</b>	0.0
11/04/13	III	0.0	1.6	<b>97.1</b>	1.3	0.0	40.8	<b>59.1</b>	0.1
20/04/13	I	<b>70.0</b>	30.0	0.0	0.0	5.2	<b>94.7</b>	0.1	0.0
27/04/13	III	0.0	21.0	<b>79.0</b>	0.0	0.1	48.2	<b>51.7</b>	0.0
03/05/13	IV	0.0	4.0	<b>53.7</b>	42.3	2.8	32.9	<b>51.5</b>	12.8
05/05/13	IV	0.0	0.0	0.0	<b>100.0</b>	0.0	0.0	23.7	<b>76.3</b>
07/05/13	IV	0.0	0.0	38.4	<b>61.6</b>	0.0	12.9	<b>85.1</b>	2.0
10/05/13	IV	0.0	0.0	46.9	<b>53.1</b>	0.0	0.3	<b>80.2</b>	19.5
15/05/13	II	6.2	<b>93.8</b>	0.0	0.0	10.3	<b>89.7</b>	0.0	0.0
19/05/13	IV	0.0	0.0	34.2	<b>65.8</b>	0.0	5.7	<b>88.8</b>	5.5
23/05/13	II	0.0	<b>100.0</b>	0.0	0.0	0.7	<b>97.3</b>	2.0	0.0
29/05/13	IV	0.0	0.3	<b>85.0</b>	14.7	0.0	21.0	<b>74.7</b>	4.3
09/06/13	IV	0.0	0.0	22.2	<b>77.8</b>	0.0	0.1	<b>67.3</b>	32.6
23/06/13	III	0.0	44.4	<b>55.5</b>	0.1	0.8	47.1	<b>51.7</b>	0.4
27/06/13	IV	0.0	0.0	<b>82.7</b>	17.3	0.0	0.9	<b>92.5</b>	6.6
07/07/13	II	13.4	<b>35.5</b>	34.7	16.4	14.0	<b>36.7</b>	34.8	14.5

## SENSITIVITY ANALYSIS

### *Sensitivity to the temporal resolution of the data*

The sensitivity of the hysteresis index  $h$  and the determination of the hysteresis classes based on  $h$  and the associated values of  $\Delta A_{\min}$  and  $\Delta A_{\max}$  to the temporal resolution of the data were analysed for the hysteretic relation between streamflow and soil moisture at the mid-hillslope (SM3) location at Ressi. To determine the sensitivity of the hysteresis index to the temporal resolution of the data, data points from the streamflow and soil moisture datasets were systematically removed to simulate measurement intervals of 10, 15, 20 and 30 min, and  $h$ ,  $\Delta A_{\min}$  and  $\Delta A_{\max}$  were computed for the events with both the original data (5-min) and the simulated lower temporal resolution data. Cohen's kappa,  $\kappa$  (Cohen, 1960), was used to assess the agreement between the classifications of the hysteretic loops with the original and the simulated data:

$$\kappa = \frac{p_o - p_e}{1 - p_e} \quad (8)$$

where  $p_o$  is the relative observed agreement among the classifications with the original and the simulated data and  $p_e$  is the relative agreement due to chance. Cohen's kappa varies between 0 (there is no agreement other than what would be expected by chance) and 1 (perfect agreement between the classifications).

Overall, the analysis reveals a very good agreement between the classification with the original and the simulated data with a different temporal resolution ( $\kappa=0.86, 0.86, 0.86$  and  $0.85$  for the agreement between the classification with the original 5-min data and the 10-, 15-, 20- and 30-min interval data, respectively). Most loops were classified similarly as for the original data (66.7% to 100% of loops identified using 10-, 15-, 20- or 30-min data were classified similar as the loops based on the original data; Table VI). Only four hysteretic loops were classified differently after decreasing the temporal resolution of the data (i.e. the rainfall-runoff events on 26 September 2012, 5 May 2013, 23 June 2013 and 7 July 2013). Two of these events (23 June 2013 and 07 July 2013) were characterized by a small change in soil moisture (only 0.25% and 0.29% for 23 June 2013 and 07 July 2013, respectively); one had a very steep rising limb (05 May 2013) with few data points on the rising limb, while the fourth event (26 September 2012) had a loop with a very complex shape. Decreasing the temporal resolution of the data for these events significantly influenced the number of data points on the rising limb and, not surprisingly, significantly affected the shape of the hysteretic loops and the calculated values of  $h$ ,  $\Delta A_{\min}$  and  $\Delta A_{\max}$ . Therefore, caution should be used when applying the index to

events with only a few measurements on the rising (or the falling) limb.

### *Sensitivity to noise in the data*

We also studied the sensitivity of the hysteresis index to instrumental error or noise in the input data. Gaussian noise was simulated independently for streamflow and soil moisture by generating arrays of pseudo-random numbers whose elements were normally distributed (mean  $\approx 0$  and variance  $\approx 1$ ). The random numbers were scaled by 1% and 5%, multiplied by the original data and then added to the original values to generate a disturbed (noisy) signal. We iterated the process 1000 times for each event and determined the hysteresis class and the value of  $h$ . The median and the interquartile ranges of  $h$  were compared with the values calculated for the original data.

Cohen's kappa results suggest that there was a good ( $\kappa=0.72$ ) and a fair ( $\kappa=0.29$ ) agreement between the classifications with the original and the 1%-scaled and 5%-scaled noisy data, respectively. The medians of  $h$  for the 1%-scaled noisy data were similar to  $h$  for the original data, but the interquartile ranges were large for some rainfall-runoff events (Figure 6). For 27 out of the 30 events, the most common hysteresis class for the simulations with 1% noise was similar to the hysteresis class obtained for the original data (79.6% of agreement between the classifications) (Table VII). Conversely, the medians of  $h$  for the 5%-scaled noisy data and the value computed for the original data were similar for some events but different for other events (Figure 6). The agreement of the classification of the hysteretic loops was also poorer than for the 1%-scaled noisy loops: the majority of the simulated loops corresponded to the classification obtained using the original data for only 16 events (44.4% of agreement between the classifications) (Table VII). The interquartile ranges of  $h$  were particularly large for rainfall-runoff events with small changes in streamflow and soil moisture and short events. These results suggest that the hysteresis index can be considered quite robust when measurement errors occur for large and long rainfall events but that the index should be used with caution when noise or errors affect the measurements during small events.

## DISCUSSION

### *Comparison with previous indices*

Several quantitative indices have been developed to characterize hysteresis in the past. Most of these indices were tested for the relation between streamflow and suspended sediment concentrations (e.g. Aich *et al.*, 2014; Lawler *et al.*, 2006; Langlois *et al.*, 2005) or streamflow and solute concentrations (e.g. Butturini *et al.*,

2006). The hysteresis index presented in this study can be used for a wide range of (hydrological) variables, making it more versatile than most of the previously developed indices. The hysteresis index is consistent with the theoretical interpretation of the direction of the loops when using dependent variables that have positive (e.g. soil moisture, water level and EC) and negative values (e.g. isotopic composition and depth to water table) that increase (e.g. soil moisture or water table) during a runoff event. There are a few similarities and substantial differences between the new index and the previous indices. The  $h$  index shares a common background with  $H$  (Langlois *et al.*, 2005) because both methods are based on the computation of definite integrals. However, our method is more robust because it does not rely on the fitted regression lines for the rising and the falling limbs of the hydrograph in the hysteretic plot (Langlois *et al.*, 2005). Noise in the data and some loop shapes (e.g. Figure 2e) can result in a poor fit of the best regression equation to the observed data, influencing the value of  $H$ . Conversely, the application of the  $h$  index is less constrained by noise in the data and can be applied to complex hysteretic loops. The interpretation of the new versatile index is also similar to the index developed by Lawler *et al.* (2006). Both indices are positive for mainly clockwise loops and negative for anticlockwise loops, providing symmetry across the range of clockwise and anticlockwise hysteretic loops. Compared with the  $HI_{\text{mid}}$  and  $HI_{\text{mean}}$  (Lawler *et al.*, 2006),  $h$  solves the possible issue of initially non-changing dependent variables and is not affected by values that are equal to zero.

The first step for the computation of the  $HI$  index of Aich *et al.* (2014) is a normalization of the data series, which is similar to the computation of our index. However, we use a minimum–maximum normalization that allows us to narrow the range of values to  $[0, 1]$ , even for variables with a negative sign. Furthermore, the  $HI$  index of Aich *et al.* (2014) relies on data at the end of the runoff event, implying a degree of subjectivity because the length and the slope of the line connecting the last point to the peak of the independent variable changes depending on when the last data point is collected. This is particularly important when hysteretic relations are examined for non-continuous data, such as water quality samples, or a new event occurs shortly after the previous event. Because multiple values of  $\Delta A_{[i,j]}$  are used for the calculation of  $h$  (i.e.  $h$  is a metric that summarizes the shape of the loops), the computation does not depend on only two observed values, especially the last sample or the end of the event.

The  $\Delta R$  index developed by Butturini *et al.* (2006) has been demonstrated to be efficient in its applications (e.g.

Bierozza and Heathwaite, 2015; Butturini *et al.*, 2006) because it relies on the direct measurement of the extent of the loops (i.e. the computation of the area) and on the rotational parameter,  $R$ , which describes the direction of the hysteresis. However,  $R$  has to be determined by visual inspection of each loop (Bierozza and Heathwaite, 2015), which limits the automatic application of the index for large datasets. Conversely, the new hysteresis index and the indices developed by Langlois *et al.* (2005), Lawler *et al.* (2006) and Aich *et al.* (2014) can easily be implemented to automatically detect the direction of hysteresis and can thus be used to analyse large datasets or to compare measurements and model results.

The tests with synthetic data (Tables II and III) were useful to compare the index we presented here to the indices developed by Langlois *et al.* (2005), Lawler *et al.* (2006) and Aich *et al.* (2014). Although the indices are based on different methods to assess the ‘fatness’ of the loops (i.e.  $h$  and  $H$  on integrals computed for the rising and the falling limbs,  $HI_{\text{mid}}$  and  $HI_{\text{mean}}$  on ratios,  $HI$  on the maximum distance between the rising and the falling limbs of the hysteretic loop and the line that links the maximum value of the independent variable to the last data point), all of them captured the change in the extent of hysteresis for simple loops (Table II). The comparison of the synthetic eight-shaped loops (Table III) showed that  $HI_{\text{mid}}$  and  $HI$  are less useful to detect differences in the shape and the extent of eight-shaped loops because they characterize hysteresis at only one point of the independent variable ( $HI_{\text{mid}}$ ) or by just two distances ( $HI$ ).

The application of the different indices to different datasets from experimental catchments (Figure 2) showed that unlike the previously developed indices, our index,  $h$ , and the associated values of  $\Delta A_{\text{min}}$  and  $\Delta A_{\text{max}}$ , can correctly identify all major hysteresis classes, including the eight-shaped loops, and is applicable to negative data and datasets where the dependent variable decreases during an event. It can even be applied when the dependent variable remains constant at the start of the event or has a value of zero. Additional conditional statements for  $HI_{\text{mid}}$  and  $HI_{\text{mean}}$  (Lawler *et al.*, 2006) and  $H$  (Langlois *et al.*, 2005), and a different normalization for  $HI$  (Aich *et al.*, 2014) could allow these indices to also correctly identify the direction of the hysteresis for dependent variables with negative values. However, the additional conditional statements would make the outcome of the indices less intuitive.

#### *Potential use and limits of the hysteresis index*

The hysteresis index presented in this study provides objective and concise information on the direction and the shape of the hysteretic loops. Clockwise, anticlockwise and eight-shaped loops are easily determined by

four computational steps. The normalization of the two variables (step 1) is needed to compare different hysteretic loops and allows for the correct interpretation of the direction of the hysteresis for different dependent variables. The computation of the definite integrals for the rising and the falling curves (step 2) and the differences between them ( $\Delta A_{[i,j]}$ ; step 3) enables the determination of the direction and the shape of the loops, while the sum of the differences (step 4) summarizes the hysteretic loop and ensures that the index is not significantly influenced by outliers. The metrics introduced in steps 3 and 4 ( $\Delta A_{[i,j]}$  and  $h$ ) can easily be related to the characteristics of the runoff event, providing insight into the factors that lead to different hysteretic loops. These metrics can thus be used to assess changes in hysteresis in long data series with multiple events or to assess model performance. The computation of the index does not require a loop to be closed, and  $h$  can be calculated for different independent-variable intervals. The index is therefore versatile and can be applied to a wide range of datasets.

The sensitivity analysis showed a high level of agreement between the classification based on the original data and the classifications obtained for data with a lower temporal resolution, suggesting that the sensitivity of the index to the temporal resolution of the measurements is low. However, caution should be used if the index is applied when only one or two measurements are available for the rising (or falling) limb. Application of the index to very noisy data (e.g. data that show large measurement errors and relatively small responses) should be performed with caution as well.

Previous studies did not test the sensitivity of the various hysteresis indices to the temporal resolution of the data or noise in the measurements. However, this is important when indices are applied to many events or different catchments to study differences in runoff responses, or when indices are used for model calibration or validation. The results obtained from the application to field data and the sensitivity analyses revealed that the index introduced here is a powerful tool for the study of long-time series and comparative analyses of different runoff events because it was not very sensitive to noisy data or the temporal resolution of the data as long as the response was large relative to the noise and there were several data points on the rising and the falling limbs of the hydrograph. Consequently, the index can be used to study the seasonal variations in hysteretic patterns (Bieroza and Heathwaite, 2015; Aich *et al.*, 2014) or to compare hysteresis at different spatial scales or for different catchments (Smith and Dragovich, 2009). The hysteresis index can also be used in the assessment of models in their ability to reproduce the internal behaviour of catchments (e.g. Fovet *et al.*, 2015). The only condition for a correct application of the index is that the independent variable has to increase from its starting value to the peak (i.e. the normalized data vary

from 0 to 1). The index can therefore be used for a wide range of hydrological studies and in other fields across the earth system sciences.

Complex events characterized by multiple peaks are approximated by one overall hysteretic pattern because the computation of the index is based on the highest peak of the independent variable. The index therefore does not quantify the hysteretic loop of each individual runoff response that interrupts the recession curve of the first event. These multiple peak events will instead be classified as complex loops. However, the user can choose to analyse the different peaks of the independent variable as separate events and the corresponding hysteretic loops separately. This allows for the analysis of changes in hysteresis with each individual rainfall pulse or sub-event.

We used the index to detect seasonal changes in the direction of hysteresis between streamflow and soil moisture for 30 rainfall–runoff events in the Ressi catchment. The results showed seasonal changes in the direction of the hysteretic relation between hillslope soil moisture and streamflow, with the streamflow peak generally occurring before peak hillslope soil moisture during dry periods and small rainfall events, and after peak soil moisture during the wet period. These observations on the hysteretic relations between hillslope soil moisture and streamflow agree with previous studies on the role of hillslopes in generating runoff during wet conditions and large rainfall events (McGlynn *et al.*, 2004; Wenninger *et al.*, 2004; Ocampo *et al.*, 2006; Penna *et al.*, 2011, 2015b; von Freyberg *et al.*, 2014) and show the value of analysing hysteretic patterns to study (changes in) hydrological processes.

## CONCLUSIONS

We present a versatile hysteresis index for the quantification of hysteretic relations between hydrological variables at the runoff event timescale. Because of the frequent occurrence of hysteresis in hydrology and other earth system sciences, various indices have been proposed in the past, particularly to describe the relation between streamflow and sediment or solute concentrations. However, the previous indices were developed for specific cases and therefore have limitations that prevent their use in a broader range of studies. Particularly, they cannot correctly identify eight-shaped loops and require additional conditional statements or normalizations to correctly identify hysteresis for variables that have a negative value (e.g. isotopic composition of stream water).

The index introduced here provides objective and concise information on the main direction of the hysteretic loop. Clockwise, anticlockwise and eight-shaped loops can be automatically determined by four



computational steps. The computation of the index does not require that the loop is closed, and the index can be calculated for different independent-variable intervals.

Tests on synthetic data and application to field data proved that  $h$ , together with the values of  $\Delta A_{\min}$  and  $\Delta A_{\max}$ , identifies the main hysteresis classes correctly. The sensitivity analysis showed a low sensitivity of the index to data with different temporal resolutions or noisy data. However, we recommend caution when using hysteresis analyses with data affected by large errors relative to the response or when the temporal resolution of the measurements is not well suited to study process dynamics.

The index was used to detect seasonal changes in the direction of the hysteretic relation between streamflow and hillslope soil moisture in the Ressi catchment, highlighting the limited role of hillslopes to streamflow during dry conditions and small events (cf. the results based on isotope hydrograph separation in Penna *et al.* (2015b)). The index can be used to test if models reproduce similar seasonal variability in hysteresis or to compare hydrological responses in different catchments or at different spatial scales.

#### ACKNOWLEDGEMENTS

The Agency for Environmental Protection (ARPAV) of Veneto Region is acknowledged for sharing the meteorological data used for the BCC and the Ressi catchment. Luca Carturan (University of Padova) is thanked for sharing the data of Noce Nero in the Alta Val de La Mare catchment. We thank Marc Vis (University of Zurich) for converting the MATLAB scripts into a user-friendly application written in Java. An anonymous reviewer and the editor are thanked for their very useful comments.

#### REFERENCES

- Aich V, Zimmermann A, Elsenbeer H. 2014. Quantification and interpretation of suspended-sediment discharge hysteresis patterns: how much data do we need? *Catena* **122**: 120–129. DOI:10.1016/j.catena.2014.06.020.
- Allen DM, Whitfield PH, Werner A. 2010. Groundwater level responses in temperate mountainous terrain: regime classification, and linkages to climate and streamflow. *Hydrological Processes* **24**: 3392–3412. DOI:10.1002/hyp.7757.
- Andermann C, Longuevergne L, Bonnet S, Crave A, Davy P, Gloaguen R. 2012. Impact of transient groundwater storage on the discharge of Himalayan rivers. *Nature Geoscience* **5**: 127–132. DOI:10.1038/NGEO1356.
- Aubert AH, Gascuel-Odoux C, Merot P. 2013. Annual hysteresis of water quality: a method to analyse the effect of intra- and inter-annual climatic conditions. *Journal of Hydrology* **478**: 29–39. DOI:10.1016/j.jhydrol.2012.11.027.
- Bieroza MZ, Heathwaite AL. 2015. Seasonal variation in phosphorous concentration–discharge hysteresis inferred from high-frequency *in situ* monitoring. *Journal of Hydrology* **524**: 333–347. DOI:10.1016/j.jhydrol.2015.02.036.
- Blaen PJ, Hannah DM, Brown LE, Milner AM. 2013. Water temperature dynamics in High Arctic river basins. *Hydrological Processes* **27**: 2958–2972. DOI:10.1002/hyp.9431.
- Briggs MA, Day-Lewis FD, Ong JB, Harvey JW, Lane JW. 2014. Dual-domain mass-transfer parameters from electrical hysteresis: theory and analytical approach applied to laboratory, synthetic streambed, and groundwater experiments. *Water Resources Research* **50**: 8281–8299. DOI:10.1002/2014WR015880.
- Burt TP, Worrall F, Howden NJK, Anderson MG. 2015. Shifts in discharge–concentration relationships as a small catchment recovers from severe drought. *Hydrological Processes* **29**: 498–507. DOI: 10.1002/hyp.10169
- Butturini A, Gallart F, Latron J, Vazquez E, Sabater F. 2006. Cross-site comparison of variability of DOC and nitrate c-q hysteresis during the autumn–winter period in three Mediterranean headwater streams: a synthetic approach. *Biogeochemistry* **77**: 327–349. DOI:10.1007/s10533-005-0711-7.
- Camporese M, Penna D, Borga M, Paniconi C. 2014. A field and modeling study of nonlinear storage–discharge dynamics for an Alpine headwater catchment. *Water Resources Research* **50**: 806–822. DOI:10.1002/2013WR013604.
- Carturan L, Cazorzi F, Dalla Fontana G. 2012. Distributed mass-balance modelling on two neighbouring glaciers in Ortles-Cevedale, Italy, from 2004 to 2009. *Journal of Glaciology* **58**: 467–486. DOI: http://dx.doi.org/10.3189/2012JG11J111
- Cartwright I, Gilfedder B, Hofmann H. 2014. Contrasts between estimates of baseflow help discern multiple sources of water contributing to rivers. *Hydrology and Earth System Sciences* **18**: 15–30. DOI:10.5194/hess-18-15-2014.
- Cohen J. 1960. A coefficient of agreement for nominal scales. *Educational and Psychological Measurement* **20**: 37–46. DOI:10.1177/001316446002000104.
- Davies JAC, Beven K. 2015. Hysteresis and scale in catchment storage, flow, and transport. *Hydrological Processes* **29**: 3604–3615. DOI:10.1002/hyp.10511.
- Detty JM, McGuire KJ. 2010a. Topographic controls on shallow groundwater dynamics: implications of hydrologic connectivity between hillslopes and riparian zones in a till mantled catchment. *Hydrological Processes* **24**: 2222–2236. DOI:10.1002/hyp.7656.
- Detty JM, McGuire KJ. 2010b. Threshold changes in storm runoff generation at a till-mantled headwater catchment. *Water Resources Research* **46**: W07525. DOI:10.1029/2009WR008102.
- Evans C, Davies TD. 1998. Causes of concentration/discharge hysteresis and its potential as a tool for analysis of episode geochemistry. *Water Resources Research* **34**: 129–137.
- Faticchi S, Katul GG, Ivanov VY, Pappas C, Paschalis A, Consolo A, Kim J, Burlando P. 2015. Abiotic and biotic controls of soil moisture spatio-temporal variability and the occurrence of hysteresis. *Water Resources Research*. DOI:10.1002/2014WR016102.
- Fovet O, Ruiz L, Hrachowitz M, Faucheux M, Gascuel-Odoux C. 2015. Hydrological hysteresis and its value for assessing process consistency in catchment conceptual models. *Hydrology and Earth System Sciences* **19**: 105–123. DOI:10.5194/hess-19-105-2015.
- Frei S, Lischeid G, Fleckenstein JH. 2010. Effects of micro-topography on surface–subsurface exchange and runoff generation in a virtual riparian wetland – a modeling study. *Advances in Water Resources* **33**: 1388–1401. DOI:10.1016/j.advwatres.2010.07.006.
- von Freyberg J, Radny D, Gall HE, Schirmer M. 2014. Implications of hydrologic connectivity between hillslopes and riparian zones on streamflow composition. *Journal of Contaminant Hydrology* **169**: 62–74. DOI: 10.1016/j.jconhyd.2014.07.005
- Haga H, Matsumoto Y, Matsutani J, Fujita M, Nishida K, Sakamoto Y. 2005. Flow paths, rainfall properties, and antecedent soil moisture controlling lags to peak discharge in a granitic unchanneled catchment. *Water Resources Research* **41**: W12410. DOI:10.1029/2005WR004236.
- Hornberger GM, Scanlon TM, Raffensperger JP. 2001. Modelling transport of dissolved silica in a forested headwater catchment: the effect of hydrological and chemical time scales on hysteresis in the concentration–discharge relationship. *Hydrological Processes* **15**: 2029–2038. DOI:10.1002/hyp.254.

- Ivanov VY, Faticchi S, Jenerette GD, Espeleta JF, Troch PA, Huxman TE. 2010. Hysteresis of soil moisture spatial heterogeneity and the “homogenizing” effect of vegetation. *Water Resources Research* **46**: W09521. DOI:10.1029/2009WR008611
- Kuppel S, Houspanossian J, Noretto MD, Jobbágy EG. 2015. What does it take to flood the Pampas? Lessons from a decade of strong hydrological fluctuations. *Water Resources Research* **51**: DOI:10.1002/2015WR016966.
- Landers MN, Sturm TW. 2013. Hysteresis in suspended sediment to turbidity relations due to changing particle size distributions. *Water Resources Research* **49**: 5487–5500. DOI:10.1002/wrcr.20394.
- Langlois JL, Johnson DW, Mehufs GR. 2005. Suspended sediment dynamics associated with snowmelt runoff in a small mountain stream of Lake Tahoe (Nevada). *Hydrological Processes* **19**: 3569–3580. DOI:10.1002/hyp.5844.
- Lawler DM, Petts GE, Foster IDL, Harper S. 2006. Turbidity dynamics during spring storm events in an urban headwater river system: the Upper Tame, West Midlands, UK. *Science of the Total Environment* **360**: 109–126. DOI:10.1016/j.scitotenv.2005.08.032.
- Mano V, Nemery J, Belleudy P, Poirel A. 2009. Assessment of suspended sediment transport in four alpine watersheds (France): influence of the climatic regime. *Hydrological Processes* **23**: 777–792. DOI:10.1002/hyp.7178.
- Mao L, Dell’Agnese A, Huincache C, Penna D, Engel M, Niedrist G, Comiti F. 2014. Bedload hysteresis in a glacier-fed mountain river. *Earth Surface Processes and Landforms* **39**: 964–976. DOI:10.1002/esp.3563.
- McGlynn BL, McDonnell JJ, Seibert J, Kendall C. 2004. Scale effects on headwater catchment runoff timing, flow sources, and groundwater–streamflow relations. *Water Resources Research* **40**: W07504. DOI:10.1029/2003WR002494.
- McGuire KJ, McDonnell JJ. 2010. Hydrological connectivity of hillslope and streams: characteristic time scales and nonlinearities. *Water Resources Research* **46**: W10543. DOI:10.1029/2010WR009341.
- Murphy JC, Hornberger GM, Liddle RG. 2014. Concentration–discharge relationships in the coal mined region of the New River basin and Indian Fork sub-basin, Tennessee, USA. *Hydrological Processes* **28**: 718–728. DOI:10.1002/hyp.9603.
- Niedzialek JM, Ogdan FL. 2004. Numerical investigation of saturated source area behavior at the small catchment scale. *Advances in Water Resources* **27**: 925–936. DOI:10.1016/j.advwatres.2004.06.005.
- Norbiato D, Borga M. 2008. Analysis of hysteretic behaviour of a hillslope-storage kinematic wave model for subsurface flow. *Advances in Water Resources* **31**: 118–131. DOI:10.1016/j.advwatres.2007.07.001.
- Ocampo CJ, Sivapalan M, Oldham C. 2006. Hydrological connectivity of upland-riparian zones in agricultural catchments: implications for runoff generation and nitrate transport. *Journal of Hydrology* **331**: 643–658. DOI:10.1016/j.jhydrol.2006.06.010.
- O’Kane JP. 2005. Hysteresis in hydrology. *Acta Geophysica Polonica* **53**: 373–383.
- Outram FN, Lloyd CEM, Jonczyk J, Benskin CMWH, Grant F, Perks MT, Deasy C, Burke SP, Collins AL, Freer J, Haygarth PM, Hiscock KM, Johnes PJ, Lovett AL. 2014. High-frequency monitoring of nitrogen and phosphorous response in three rural catchments to the end of the 2011–2012 drought in England. *Hydrology and Earth System Sciences* **18**: 3429–3448. DOI:10.5194/hess-18-3429-2014.
- Parajka J, Naeimi V, Blöschl G, Wagner W, Merz R, Scipal K. 2006. Assimilating scatterometer soil moisture data into conceptual hydrologic models at the regional scale. *Hydrology and Earth System Sciences* **10**: 353–368. DOI:10.5194/hess-10-353-2006.
- Penna D, Mantese N, Hopp L, Dalla Fontana G, Borga M. 2015a. Spatio-temporal variability of piezometric response on two steep alpine hillslopes. *Hydrological Processes* **29**: 198–211. DOI:10.1002/hyp.10140.
- Penna D, van Meerveld HJ, Oliviero O, Zuecco G, Assendelft RS, Dalla Fontana G, Borga M. 2015b. Seasonal changes in runoff generation in a small forested mountain catchment. *Hydrological Processes* **29**: 2027–2042. DOI:10.1002/hyp.10347.
- Penna D, Tromp-van Meerveld HJ, Gobbi A, Borga M, Dalla Fontana G. 2011. The influence of soil moisture on threshold runoff generation processes in an alpine headwater catchment. *Hydrology and Earth System Sciences* **15**: 689–702. DOI:10.5194/hess-15-689-2011.
- Phillips JD. 2003. Sources of nonlinearity and complexity in geomorphic systems. *Progress in Physical Geography* **27**: 1–23. DOI:10.1191/0309133303pp340ra.
- Poggi-Varaldo HM, Rinderknecht-Seijas N. 2003. A differential availability enhancement factor for the evaluation of pollutant availability in soil treatments. *Acta Biotechnologica* **23**: 271–280. DOI:10.1002/abio.200390034.
- Prowse CW. 1984. Some thoughts on lag and hysteresis. *Area* **16**: 17–23.
- Sander GC, Zheng T, Heng P, Zhong Y, Barry DA. 2011. Sustainable soil and water resources: modeling soil erosion and its impact on the environment. In Chan, F., Marinova, D. and Anderssen, R.S. (eds) MODSIM2011, 19th International Congress on Modelling and Simulation. Modelling and Simulation Society of Australia and New Zealand, December 2011, 1652–1658. ISBN: 978-0-9872143-1-7.
- Shanley JB, Sebestyen SD, McDonnell JJ, McGlynn BL, Dunne T. 2015. Water’s Way at Sleepers River watershed – revisiting flow generation in a post-glacial landscape, Vermont USA. *Hydrological Processes* **29**: 3447–3459. DOI:10.1002/hyp.10377.
- Shook KR, Pomeroy JW. 2011. Memory effects of depression storage in Northern Prairie hydrology. *Hydrological Processes* **25**: 3890–3898. DOI:10.1002/hyp.8381.
- Smith HG, Dragovich D. 2009. Interpreting sediment delivery processes using suspended sediment-discharge hysteresis patterns from nested upland catchments, south-eastern Australia. *Hydrological Processes* **23**: 2415–2426. DOI:10.1002/hyp.7357.
- Spence C. 2010. A paradigm shift in hydrology: storage thresholds across scales influence catchment runoff generation. *Geography Compass* **4**: 819–833. DOI:10.1111/j.1749-8198.2010.00341.x.
- Subehi L, Fukushima T, Onda Y, Mizugaki S, Gomi T, Kosugi K, Hiramatsu S, Kitahara H, Kuraji K, Terajima T. 2010. Analysis of stream water temperature changes during rainfall events in forested watersheds. *Limnology* **11**: 115–124. DOI:10.1007/s10201-009-0296-2.
- Visintin A. 2006. Quasilinear parabolic P.D.E.s with discontinuous hysteresis. *Annali di Matematica Pura ed Applicata* **185**: 487–519. DOI:10.1007/s10231-005-0164-6.
- Wenninger J, Uhlenbrook S, Tilch N, Leibundgut C. 2004. Experimental evidence of fast groundwater responses in a hillslope/floodplain area in the Black Forest Mountains, Germany. *Hydrological Processes* **18**: 3305–3322. DOI:10.1002/hyp.5686.
- Wetzel K. 2003. Runoff production processes in small alpine catchments within the unconsolidated Pleistocene sediments of the Lainbach area (Upper Bavaria). *Hydrological Processes* **17**: 2463–2483. DOI:10.1002/hyp.1254.
- Wilby RL, Johnson MF, Toone JA. 2014. Nocturnal river water temperatures: spatial and temporal variations. *Science of the Total Environment* **482–483**: 157–173. DOI:10.1016/j.scitotenv.2014.02.123.
- Zhang Q, Manzoni S, Katul G, Porporato A, Yang D. 2014. The hysteretic evapotranspiration–vapor pressure deficit relation. *Journal of Geophysical Research, Biogeosciences* **119**: 125–140. DOI:10.1002/2013JG002484.
- Zheng H, Wang Q, Zhu X, Li Y, Yu G. 2014. Hysteresis responses of evapotranspiration to meteorological factors at a diel timescale: patterns and causes. *PloS One* **9**(6): e98857. DOI:10.1371/journal.pone.0098857.

## SUPPORTING INFORMATION

Additional supporting information may be found in the online version of this article at the publisher’s website.